Biosensors and Bioelectronics 87 (2017) 638–645

Contents lists available at ScienceDirect

Biosensors and Bioelectronics

journal homepage: www.elsevier.com/locate/bios

A novel upconversion@polydopamine core@shell nanoparticle based aptameric biosensor for biosensing and imaging of cytochrome *c* inside living cells

Lina Ma [a], Fuyao Liu [a,b], Zhen Lei [a,b], Zhenxin Wang [a,*]

[a] State Key Laboratory of Electroanalytical Chemistry, Changchun Institute of Applied Chemistry, Chinese Academy of Sciences, Changchun 130022, PR China
[b] University of Chinese Academy of Sciences, No.19A Yuquan Road, Beijing 100049, PR China

ARTICLE INFO

Article history:
Received 17 June 2016
Received in revised form
16 August 2016
Accepted 5 September 2016
Available online 6 September 2016

Keywords:
Upconverting nanoparticles
Polydopamine nanoparticles
Aptameric biosensor
Cytochrome *c*
Living cell imaging
Intracellular quantitative analysis

ABSTRACT

Herein, a novel upconversion@polydopamine core@shell nanoparticle (termed as UCNP@PDA NP) -based aptameric biosensor has been fabricated for the quantitative analysis of cytochrome *c* (Cyt *c*) inside living cells, which comprises an UCNP@PDA NP, acting as an internal reference and fluorescence quenching agent, and Cy3 modified aptamer enabling ratiometric quantitative Cyt *c* measurement. After the hybridization of Cy3 labeled aptamer with amino-terminated single DNA on the UCNP@PDA NP surface (termed as UCNP@PDA@AP), the fluorescence of Cy3 can be efficiently quenched by the PDA shell. With the spontaneous cellular uptake of UCNP@PDA@AP, the Cyt *c* aptamer dissociates from UCNP@PDA NP surface through formation of aptamer-Cyt *c* complex, resulting in concomitant activation of the Cy3 fluorescence. High amount of Cyt *c* leads to high fluorescence emission, enabling direct visualization/measurement of the Cyt *c* by fluorescence microscopy/spectroscopy. The steady upconversion luminescent (UCL) signals can be employed not only for intracellular imaging, but also as an internal reference for evaluating intracellular Cyt *c* amount using the ratio of fluorescence intensity of Cy3 with the UCL intensity of UCNP. The UCNP@PDA@AP shows a reasonable detection limit (20 nM) and large dynamic range (50 nM to 10 μM, which covers the literature reported values (1–10 μM) for cytosolic Cyt *c* in apoptotic cells) for detecting Cyt *c* in buffer with excellent selectivity. In addition, the UCNP@PDA@AP has been successfully used to monitor etoposide induced intracellular releasing of Cyt *c*, providing the possibility for cell-based screening of apoptosis-inducing drugs.

1. Introduction

As an important biomarker for the early stage of apoptosis, cytochrome *c* (Cyt *c*) is recognized as a key component of the intrinsic apoptotic pathway, and often defined the point of no-return in cell apoptosis (Degterev et al., 2003; Green and Kroemer, 2004; Martinou, 1999; Li et al., 2015). Monitoring and detecting Cyt *c* released by mitochondria into the cytoplasm in living cells can lead to a better understanding of certain diseases on a cellular level and screen anti-cancer drug from potential candidates which induce apoptosis in cancer cells (Chen et al., 2015; Cao et al., 2009; Shen et al., 2008; Loo et al., 2014). A variety of assays have already been developed for Cyt *c* detection including the enzyme-linked immune sorbent assay (ELISA), Western blot analysis, instrument-dependent methods (e.g., mass spectrometry, high-pressure liquid chromatography (HPLC) and inductively coupled plasma mass spectrometry (ICP-MS)), and optical and/or electrochemical biosensors (Guo et al., 2015; Pandiaraj et al., 2014, 2013; Liu and Yan, 2011; Li et al., 2010; del Valle-Mondragón et al., 2008; Crouser et al., 2003; Luo and Huang, 2009; Waterhouse and Trapani, 2003; van Beek-Harmsen and van der Laarsem, 2005). Though possessing high sensitivity, most of these methods are not suitable for detecting Cyt *c* in living cell because they normally require lysis or immobilization of cell samples (Uren et al., 2005; Trusova et al., 2010). Currently, green fluorescent protein (GFP)- or tetracysteine-based assays are widely employed for live-cell tracking of Cyt *c* translocation, which require tedious operations to derive cell lines expressing Cyt *c* fusions (Waterhouse and Trapani, 2003; Goldstein et al., 2005). Very recently, an aptameric nanosensor has been firstly developed for fluorescence activation imaging of Cyt *c* released from mitochondria by assembly of a fluorophore-tagged DNA aptamer on PEGylated graphene nanosheets (Chen et al., 2015). Although a variety of assays have already been developed for detecting Cyt *c*, it is still a challenge to quantitative analysis and/or semiquantitative analysis of Cyt *c* in living cells.

* Corresponding author.
E-mail address: wangzx@ciac.ac.cn (Z. Wang).

http://dx.doi.org/10.1016/j.bios.2016.09.017
0956-5663/

Rare-earth (RE) ions doped upconverting nanoparticles (UCNPs) have been of considerable interest in recent years since UCNPs exhibit excellent photostability, for instance they display neither photoblinking on the millisecond and second time scales nor photobleaching even with hours of continuous excitation (Park et al., 2015). Moreover, UCNPs are near-infrared (NIR) excitable, which allows for optical imaging of deeper tissues and complicated biological samples with greatly suppressed autofluorescence, and produces increased image contrast (Peng et al., 2015; Wang and Liu, 2009; Haase and Schäfer, 2011; Auzel, 2004; Li et al., 2012). Among upconverting nanomaterials, the hexagonal-phase $NaYF_4$ crystal host lattice doped with lanthanide combinations of Yb^{3+}, Er^{3+} has shown excellent upconversion luminescence (UCL) (Gu et al., 2013). For application of UCNPs in the bioanalytical/biomedical fields, surface coating procedure is normally employed to transfer hydrophobic UCNPs into aqueous solution (Ju et al., 2012; Li et al., 2013; Liu et al., 2010, 2012; Zhou et al., 2010). We have successfully prepared bioinspired polydopamine (PDA) coated UCNPs for multimodality imaging via water-in-oil microemulsion method (Liu et al., 2015). The PDA shell not only provides active surface for further improve the functionality of UCNP, but also has the fluorescence quenching capacity equivalent to that of graphene oxide (Liu et al., 2013a, 2013b, 2013c; Ma et al., 2015; Qiang et al., 2014; Lin et al., 2014). In addition, PDA shell can efficiently inhibit nuclease digestion of DNA absorbed on its surface which makes PDA shell as a good DNA carrier under physiological conditions (Ma et al., 2015; Lin et al., 2014).

Herein, we developed an UCNP@PDA core@shell nanoparticle (termed as UCNP@PDA NP)-based fluorescence activated aptameric biosensor for intracellular quantitative analysis of Cyt *c*. In this case, UCNP@PDA NP acts as an internal reference and fluorescence quenching agent while Cy3 modified aptamer enables ratiometric quantitative Cyt *c* measurement.

2. Experimental section

2.1. Materials and reagents

Rare-earth oxides including gadolinium oxide (Gd_2O_3, 99.99%), ytterbium oxide (Yb_2O_3, 99.99%), erbium oxide (Er_2O_3, 99.99%), yttrium oxide (Y_2O_3, 99.99%), dopamine hydrochloride (99%), and ammonium hydroxide (28.0–30.0% NH_3 by weight) were obtained from Alfa Aesar Co. (Ward Hill, USA). 1-Octadecene (ODE, 90%), oleic acid (OA, 90%), cytochrome *c* (Cyt *c*), etoposide, human serum albumin (HSA), immunoglobulin G (IgG), bovine serum albumin (BSA), isoascorbic acid (AA), glutathione (GSH) and L-tryptophane (L-Trp) were purchased from Sigma-Aldrich Co. (St Louis, USA). The Cyt *c* aptamer and the complementary DNA (cDNA) were synthesized from Sangon Biotech Ltd. (Shanghai, China). Dulbesso's modified Eagle's medium (DMEM) and fetal bovine serum (FBS) were obtained from Gibco Inc. (New York, USA). Ammonium fluoride (98%), 3-(4,5-dimethylthiazol-2-yl)-2,5-diphenyltetrazolium bromide (MTT) and Cyt *c* ELISA kit were received from Beijing Dingguo Biotechnology Ltd (Beijing, China). Hoechst 33342 and mitochondria fluorescent trackers (Mito@tracker) were obtained from Invitrogen (Carlsbad, USA). Other reagents (analytical grade) were purchased from Beijing Chemical Reagents Co. (Beijing, China). All reagents were used without further purification. Milli-Q water (18.2 MΩ cm) was used in all experiments.

2.2. Characterizations

Transmission electron microscope (TEM) micrographs were performed on a JEM 2000FX (JEOL Ltd, Japan) microscope operated at an accelerating voltage of 120 kV. The fourier transform infrared (FTIR) spectra were recorded on a Bruker Vertex 70 spectrometer (Bruker, Germany). X-ray photoelectron spectra (XPS) measurements were conducted with a VG ESCALLAB MKII spectrometer (VG, UK). Zeta potential and hydrodynamic size measurements were carried out on Malvern Zetasizer Nano ZS (Malvern Instruments Ltd, UK). Fluorescence emission spectra were recorded on a QE65 Pro fiber optic spectrometer (Ocean Optics, USA). The UCL spectra were collected on an F-4500 spectrophotometer (Hitachi Co., Japan) using an external CW NIR laser (980 nm, BWT Beijing Ltd., China) as exciting wavelength. The UCL imaging experiments were performed with a reconstructive Nikon Ti-S fluorescent microscope equipped with an infrared laser at 980 nm (BWT Beijing Ltd, China).

2.3. Synthesis of $NaYF_4$: Yb^{3+}, Er^{3+}@$NaCdF_4$ UCNPs

The $NaYF_4$: Yb^{3+}, Er^{3+} UCNPs were prepared by a previously reported procedure (Liu et al., 2013a, 2013b, 2013c). Generally, Y_2O_3, Yb_2O_3 and Er_2O_3 were reacted with excess hydrochloric acid to form the rare-earth chloride compounds, respectively. Then, the rare-earth chloride compounds were dried by solvent evaporation, and redispersed in water to yield the YCl_3 (1.6 M), $YbCl_3$ (0.6 M), and $ErCl_3$ (0.1 M) aqueous stock solutions, respectively. Subsequently, 0.5 mL YCl_3 (1.6 M), 0.3 mL $YbCl_3$ (0.6 M) and 0.2 mL $ErCl_3$ (0.1 M) aqueous solutions were mixed well in a 100 mL flask, and dried by heating. Then, 6 mL oleic acid and 15 mL 1-octadecene were added into the flask. The mixture was heated to 150 °C under Ar atmosphere to yield a homogeneous solution. After cooling to room temperature, 10 mL methanol solution containing 4 mmol NH_4F and 2.5 mmol NaOH was slowly added into the mixture with vigorous stirring. After vigorous stirring for 60 min, the solution was slowly heated to 70 °C to evaporate the methanol, and degassed at 100 °C for 10 min. Subsequently, the temperature was increased to 300 °C at a rate of 10 °C min^{-1} and remained at this temperature for 60 min. After cooling to room temperature in ambient conditions, the UCNPs were collected by centrifugation at 10,000 rpm for 10 min, and washed with ethanol (10 mL, three times). Finally, the as-prepared $NaYF_4$: Yb^{3+}, Er^{3+} UCNPs were redispersed in 10 mL cyclohexane.

The $NaGdF_4$ shell was synthesized according to a published literature with a few modifications (Liu et al., 2013a, 2013b, 2013c). In brief, $GdCl_3$ (0.5 mL, 1.0 M) was added in a 100 mL flask, and dried by heating. Then, oleic acid (4 mL) and 1-octadecene (16 mL) were added into the flask. The mixture was heated to 150 °C under Ar atmosphere to yield a homogenous solution. After cooling to 80 °C, $NaYF_4$: Yb^{3+}, Er^{3+} UCNPs (1.5 mmol) in cyclohexane (10 mL) were added to the above mixture. After removal of cyclohexane by evaporation, methanol solution (10 mL) containing NH_4F (1.375 mmol) and NaOH (1.25 mmol) was added and stirred at 50 °C for 30 min. The methanol was evaporated off and the solution was degassed for 10 min. Subsequently, the temperature of the mixture was increased to 280 °C at a rate of 10 °C min^{-1} and incubated at 280 °C for 90 min. After cooling to room temperature in ambient conditions, the as-prepared UCNPs (named as $NaYF_4$: Yb^{3+}, Er^{3+}@$NaCdF_4$ UCNPs) were collected by centrifugation (10,000 rpm for 10 min), and washed with ethanol (10 mL, three times). Finally, the $NaYF_4$: Yb^{3+}, Er^{3+}@$NaCdF_4$ UCNPs were redispersed in 10 mL cyclohexane.

2.4. Synthesis of UCNP@PDA NPs and cDNA functionalized UCNP@PDA NPs

UCNP@PDA NPs were synthesized according to our previously reported method (Liu et al., 2015). Typically, the as-prepared $NaYF_4$: Yb^{3+}, Er^{3+}@$NaCdF_4$ UCNP was redispersed in cyclohexane. For synthesizing PDA-coated UCNP with 5 nm PDA shell, Igepal

CO-520 (0.65 mL) was added in cyclohexane (10 mL) containing oleic-acid-stabilized $NaYF_4$: Yb^{3+}, Er^{3+}@$NaCdF_4$ UCNP (10 mg). After stirred for 20 min, ammonium hydroxide (75 μL, 28 wt% in water) was added into mixture followed by ultrasonic treatment for 15 min. After stirred for another 30 min, dopamine hydrochloride aqueous solution (50 μL, 25 wt%) was injected into the above reaction mixture at a rate of 3 μL min^{-1}. After stirred for 24 h, the NPs were precipitated by adding ethanol, collected by centrifugation (10,000 rpm for 10 min) and washed with ethanol and water (10 mL, three times). Finally, the UCNP@PDA NPs were redispersed in water and dried by vacuum evaporation.

Finally, the as-prepared UCNP@PDA NPs (25 mg) were reacted with cDNA (5 nmol) in 50 mL TB (Tris buffer, 10 mM, pH 8.5) under vigorous stirring for 12 h. Then, DNA functionalized UCNP@PDA NPs were purified by centrifugation (10,000 rpm, 50 mL H_2O, three times), and redispersed in water.

2.5. Sensitivity and selectivity of the biosensor in buffer

In order to obtain UCNP@PDA NP based aptameric biosensor (termed as UCNP@PDA@AP), 100 μg/mL cDNA functionalized UCNP@PDA NPs were hybridized with 10 nM Cyt *c* aptamer in PBS buffer (10 mM NaH_2PO_4/Na_2HPO_4, 137 mM NaCl, 2.7 mM KCl, pH 7.4) at 37 °C for 30 min. Under this condition, there are ca. 9 aptamer molecules on single cDNA functionalized UCNP@PDA NP (see supporting information for details). Then, the proposed UCNP@PDA@AP was incubated with various concentrations of Cyt *c* at 37 °C for another 20 min. Finally, the fluorescence spectra of the mixture were recorded on a QE65 Pro fiber optic spectrometer at the excitation wavelength of 530 nm. The UCL spectra were collected on an F-4500 spectrophotometer using an external CW NIR laser at the excitation wavelength of 980 nm.

The selectivity of UCNP@PDA@AP was examined by incubation with Cyt *c* (1 μM) and other components (10 μM) possibly coexisting with Cyt *c* at 37 °C for 20 min, respectively.

2.6. Cell culture and MTT assay of UCNP@PDA@AP

The HepG-2 cells were cultured with 100 μL fresh culture medium (fresh DMEM supplemented with 10% fetal bovine serum and 100 U/mL penicillin – streptomycin) in 96 well microtiter plate (8×10^3 cells per well) under a humidified 5% CO_2 at 37 °C for 24 h. After washed with 100 μL fresh DMEM (3 times), 100 μL fresh culture medium with various concentrations (20, 40, 60, 80 and 100 μg mL^{-1}) of UCNP@PDA@AP were added and incubated at same conditions for another 24 h, respectively. Subsequently, the cells were washed with 100 μL PBS (3 times), and then 10 μL MTT (5 mg/mL in PBS) and 100 μL cell culturing solution were added into each well and incubated for another 4 h. Finally, the supernatant was discharged, and purple formazan product was dissolved by DMSO (100 μL per well) with gentle shaking for 10 min. The absorbance of each well was read on a Power Wave XS 2 Microplate Spectrophotometer at 510 nm. The relative cell viabilities (%) were calculated by using the optical densities with respect to the control value. HepG-2 cells cultured without UCNP@PDA@AP were used as control sample.

2.7. Intracellular imaging and UCL spectra assay

The cells were seeded at a density of 1.5×10^5 cells per well in six-well culture plate with 22 mm × 22 mm glass coverslip at the bottom of well and grown in 1.5 mL fresh culture medium for 24 h. After washed with 1.5 mL fresh DMEM (3 times), the cells were incubated with 100 μg mL^{-1} UCNP@PDA@AP in 1.5 mL fresh DMEM at 37 °C for another 2 h. After washed with 1.5 mL cold PBS (3 times), the UCNP@PDA@AP stained cells were treated by various concentrations of etoposide (0, 0.5, 1, 2 and 5 μM) in 1.5 mL DMEM at 37 °C for 2 h or treated by 2 μM etoposide in 1.5 mL DMEM at 37 °C for different times (0, 1.5, 2 and 3 h), respectively. For addressing the dissociated Cy3 modified aptamer localization, the etoposide treated cells were continuously incubated with 4 μg/mL Hoechst 33342 for 5 min and 100 nM Mito@tracker red for 20 min, respectively. After washed with 1.5 mL cold PBS (3 times), the UCNP@PDA@AP stained cells were subjected to image by a reconstructive Nikon Ti-S fluorescent microscope with exiting wavelengths at 530 nm for Cy3 channel and 980 nm for UCL channel. For fluorescence and UCL spectral measurements, UCNP@PDA@AP stained cells were detached from the coverslips by 0.02% (w/v) EDTA, concentrated by centrifugation (1440*g*, 5 min) and redispersed in 1.5 mL PBS, respectively. The fluorescence spectra of UCNP@PDA@AP stained cells were measured on a QE65 Pro fiber optic spectrometer with 530 nm as the exciting wavelength. The UCL spectra of UCNP@PDA@AP stained cells were measured on a F-4500 fluorescence spectrophotometer using an external CW NIR laser with 980 nm as the exciting wavelength.

3. Results and discussion

3.1. Fabrication of the biosensor and sensing principle of intracellular Cyt c

The realization of the biosensor is illustrated in Scheme 1. The $NaGdF_4$ coated Yb and Er co-doped $NaYF_4$: Yb^{3+}, Er^{3+} were synthesized by literature reported method because the UCNP with core@shell structure has relative high upconversion fluorescence efficiency (Burns, 1965; Mai et al., 2007; Qian and Zhang, 2008). The UCNP@PDA NPs were obtained by reaction of dopamine monomers with hydrophobic $NaYF_4$: Yb^{3+}, Er^{3+}@$NaGdF_4$ UCNPs in the water-in-oil microemulsion. The as-prepared UCNP@PDA NPs were further functionalized by reacting with amino-terminated single DNA (cDNA, 5′-NH_2-TTTTGCAACAACG-3′) through Michael addition and/or Schiff base reaction (Liu et al., 2015). The UCNP@PDA NP-based fluorescence activated aptameric biosensor for Cyt *c* detection (termed as UCNP@PDA@AP) was generated by hybridization of the Cy3 labeled Cyt *c* aptamer (5′-CCGTGTCTGGGGCCGACCGGCGCATTGGGTACGTTGTTGC-Cy3-3′) with cDNA on the UCNP@PDA NP surface (Li et al., 2008). After hybridization, the fluorescence of Cy3 can be efficiently quenched by the PDA shell. With the spontaneous cellular uptake of UCNP@PDA@AP, the Cyt *c* aptamer interacts with Cyt *c* and dissociates from UCNP@PDA NP surface through formation of aptamer-Cyt *c* complex, resulting in concomitant activation of the Cy3 fluorescence. High amount of Cyt *c* leads to high fluorescence emission, enabling direct visualization/measurement of the Cyt *c* by fluorescence microscopy/spectroscopy. Due to the autofluorescence-free nature of UCNP, the steady upconversion luminescent (UCL) signals can be employed not only for intracellular imaging, but also as an internal reference for evaluating intracellular Cyt *c* amount using the ratio of fluorescence intensity of Cy3 with the UCL intensity of UCNP.

3.2. Characterization of the as-prepared NPs

The morphologies of $NaYF_4$: Yb^{3+}, Er^{3+} UCNP, $NaYF_4$: Yb^{3+}, Er^{3+}@$NaGdF_4$ UCNP and UCNP@PDA NP are characterized by transmission electron microscope (TEM). As shown in Fig. 1, the size of $NaYF_4$: Yb^{3+}, Er^{3+}@$NaGdF_4$ UCNP is ca. 50 nm in diameter which contains a $NaYF_4$: Yb^{3+}, Er^{3+} core (35 nm in diameter) and a $NaGdF_4$ shell (7.5 nm in thickness). 5 nm thickness of PDA shell is obtained by the water-in-oil method. The UCNP displays three major UCL peaks at 526, 546, and 660 nm, which are attributed to

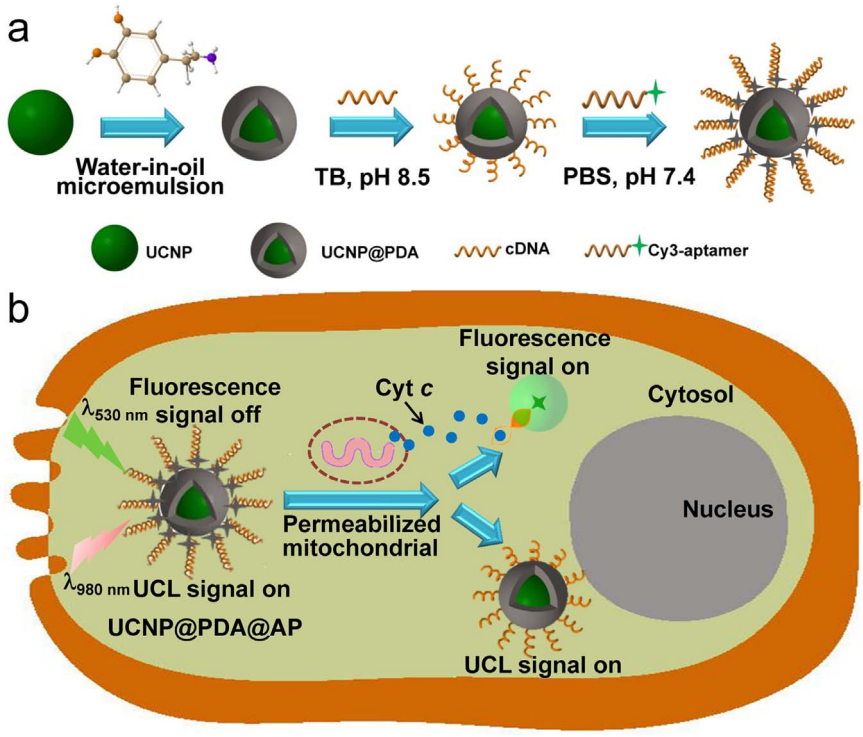

Scheme1. Illustration of (a) the UCNP@PDA@AP fabrication and (b) its application for sensing intracellular Cyt *c*. The illustration is not drawn to scale.

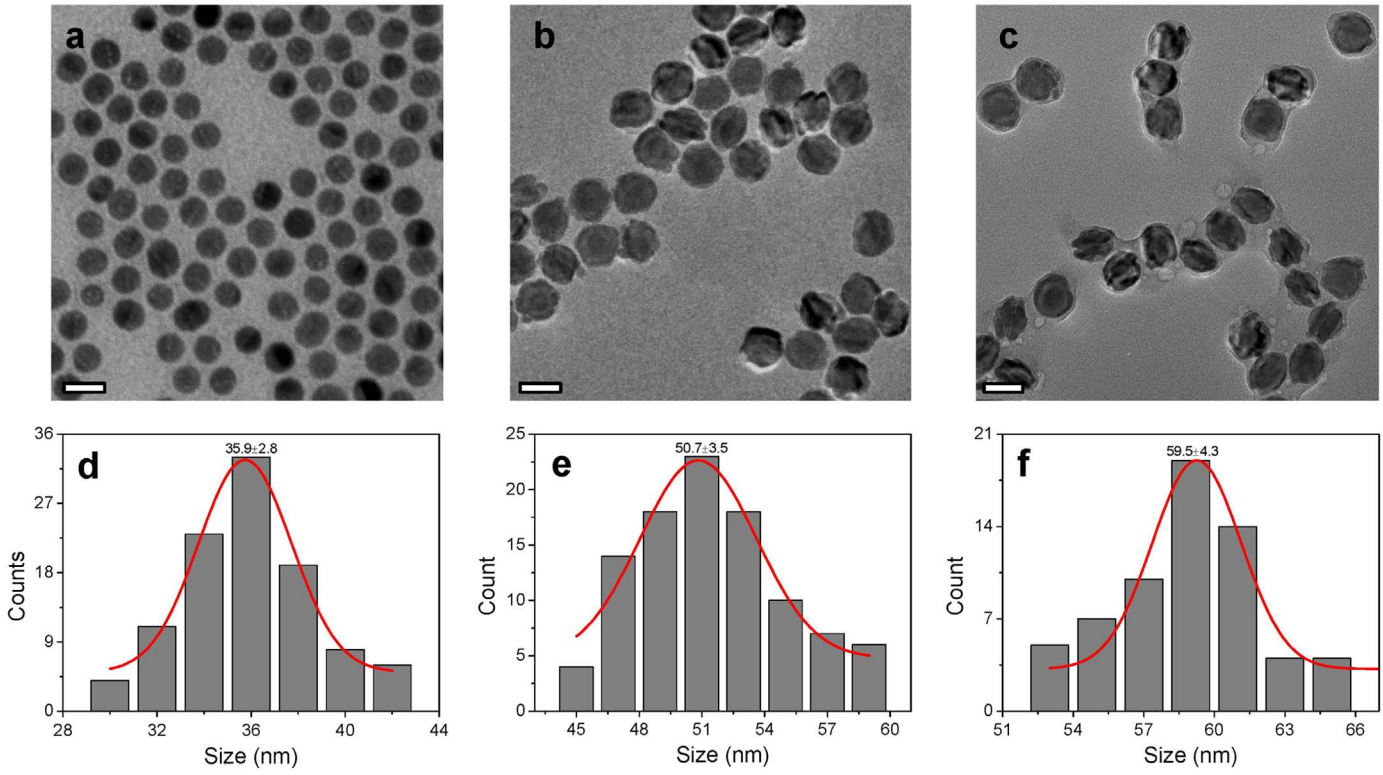

Fig. 1. TEM micrographs of (a) $NaYF_4$: Yb^{3+}, Er^{3+} UCNP, (b) $NaYF_4$: Yb^{3+}, Er^{3+}@$NaGdF_4$ UCNP, and (c) UCNP@PDA NP, respectively. The scale bars are 50 nm. (d–f) The corresponding size and size distribution of the three types of NPs (*a*-c).

the energy transitions from $^2H_{11/2}$, $^4S_{3/2}$, and $^4F_{9/2}$ to $^4I_{15/2}$ of Er^{3+} ions, respectively (Li et al., 2009). As expected, the UCL intensity of $NaYF_4$: Yb^{3+}, Er^{3+}@$NaGdF_4$ UCNP is approximately ten times higher than that of $NaYF_4$: Yb^{3+}, Er^{3+} UCNP (as shown in Fig. S1a). The UCL emission of UCNP@PDA NP is decreased slightly which was attributed to the fluorescence quenching ability of PDA shell. The FT-IR spectrum of as-prepared $NaYF_4$: Yb^{3+}, Er^{3+}@$NaGdF_4$ UCNP exhibits two IR bands at 1464 cm^{-1} and 1564 cm^{-1}, which are assigned to the -COOH stretching vibration (as shown in Fig. S1b). The experimental result indicates that oleic acid molecules are attached on the UCNP surface during NPs synthesis. For transferring the hydrophobic oleic acid capped UCNPs to aqueous

solution, PDA shell is coated on the UCNPs because the polar groups of PDA, such as hydroxyl and amine groups, endow the UCNPs with improved hydrophilicity and stability. The UCNP@PDA NPs have three IR bands at 3385 cm^{-1} (NH stretching), 1588 cm^{-1} (C=C aromatic ring stretching vibration), and 1511 cm^{-1} (NH bending), which demonstrate the presence of PDA on UCNP (as shown in Fig. S1b). The cDNA was then conjugated on UCNP@PDA NP surface through the reaction of terminal amine group of cDNA with quinone group of PDA under weak basic condition. The enhanced IR band at 1151 cm^{-1} (the C-N glucosidic bond of furanoses in DNA chain) demonstrates that the cDNA has conjugated to the UCNP@PDA NP successfully (as shown in Fig. S1b) (Zhang et al., 2014). The N1s peak can be clearly observed in the XPS spectrum of UCNP@PDA NP, which further confirms the successfully coating PDA shell on $NaYF_4$: Yb^{3+}, Er^{3+}@$NaGdF_4$ UCNP (as shown in Fig. S1c and S1d). In addition, the zeta potential of cDNA conjugated UCNP@PDA NP is lower than that of UCNP@PDA NP (as shown in Table S1). The experimental result further indicates the conjugation of cDNA on the UCNP@PDA NP surface.

3.3. Sensitivity and selectivity of UCNP@PDA@AP in buffer

The fluorescence intensity of Cy3 labeled Cyt *c* aptamer is decreased significantly after incubation with cDNA modified UCNP@PDA NP. The experimental result indicates that the Cyt *c* aptamer can efficiently hybridize with immobilized cDNA on the UCNP@PDA surface and the fluorescence emission of Cy3 can be quenched significantly by the UCNP@PDA NP through the FRET between Cy3 (donor) and PDA (acceptor) (Liu et al., 2013a, 2013b, 2013c; Ma et al., 2015; Qiang et al., 2014; Lin et al., 2014). The as-prepared UCNP@PDA@AP can be re-dispersed in different media (e.g., H_2O, PBS (10 mM NaH_2PO_4/Na_2HPO_4, 137 mM NaCl, pH 7.4), DMEM, various pH values of PBS (137 mM NaCl) and PBS containing various concentrations of NaCl (pH 7.4)). The UCNP@PDA@AP show slight changes of hydrodynamic size and maxium fluorescence emission intensity after stored under chamber conditions for 12 h (as shown in Figs. S2 and S3). The experiment results indicate that UCNP@PDA@AP has good colloidal and optical stability. Several possible influences on the fluorescence emission of UCNP@PDA@AP have investigated. The ionic strength and solution component have no obvious effect on the fluorescence emission intensity of UCNP@PDA@AP (as shown in Fig. S3). Because of protein adsorption, the UCNP@PDA@AP has relative large hydrodynamic size and red-shift of maxium emission wavelength in DMEM (as shown in Figs. S2 and S3). However, the fluorescence emission intensity of UCNP@PDA@AP is increased with increasing pH values because the optical properties of Cy3 are sensitive to the pH value (Zhao et al., 1989). The phenomenon has slightly effect on the Cyt *c* detection since the intracellular pH value is normally kept as constant.

The fluorescence intensity of Cy3 is increased proportionally with the increasing concentration of Cyt *c* (as shown in Fig. 2a). The F_R shows a linear correlation with the logarithm of the Cyt *c* concentration within the ranges from 50 nM to 10 μM, which covers the literature reported values (1–10 μM) for cytosolic Cyt *c* in apoptotic cells (as shown in Fig. 2c) (Chen et al., 2015). Here, $F_R = \Delta F_{Cy3}/F_{UCNP660}$, ΔF_{Cy3} is the difference of the fluorescence intensities of Cy3-aptamer in the presence or the absence of the

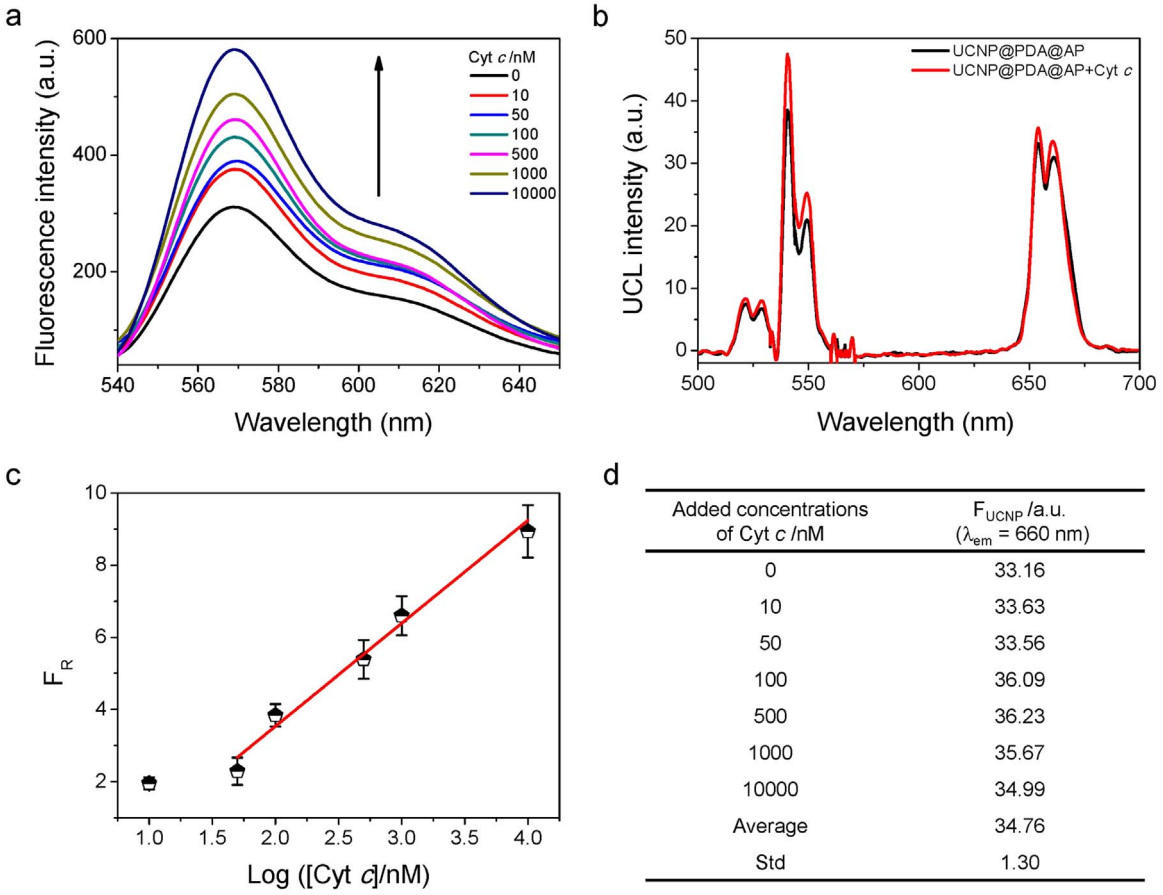

Added concentrations of Cyt *c* /nM	F_{UCNP} /a.u. (λ_{em} = 660 nm)
0	33.16
10	33.63
50	33.56
100	36.09
500	36.23
1000	35.67
10000	34.99
Average	34.76
Std	1.30

Fig. 2. (a) Fluorescence spectra of Cy3 in the presence of various concentrations of Cyt *c*. (b) UCL spectra of UCNP@PDA@AP without or with 1 μM Cyt *c*, respectively. (c) The calibration curve of F_R versus logarithm of Cyt *c* concentration. The error bars mean standard deviations ($n=6$). (d) The corresponding UCL intensities of UCNP@PDA@AP with various concentrations of Cyt *c* at the emission wavelength (λ_{em}) of 660 nm.

Cyt *c*. $F_{UCNP660}$ represents the UCL intensity of UCNP at the emission wavelength (λ_{em}) of 660 nm. The $F_{UCNP660}$ can be served as the internal reference since $F_{UCNP660}$ is not affected by the Cyt *c* (as shown in Fig. 2b and d). The detection limits (3 times the standard deviation of F_R of control sample) is 20 nM.

Other components such as human serum albumin (HSA), immunoglobulin G (IgG), bovine serum albumin (BSA), isoascorbic acid (AA), glutathione (GSH) and L-tryptophane (L-Trp) possibly coexist with Cyt *c* in real sample, which may cause accuracy problems in the Cyt *c* determination. The F_R of Cyt *c* is much higher than those of interferences (as shown in Fig. S4). The results show that the foreign substances do not interfere significantly on the Cyt *c* determination, i.e., the UCNP@PDA@AP presents good selectivity on the Cyt *c* detection.

3.4. Living cell imaging of Cyt c

The Cytotoxicity of UCNP@PDA@AP is investigated using HepG-2 cell line (human liver carcinoma cell line). After incubated with cells for 24 h, the UCNP@PDA@AP shows a negligible cytotoxicity as high as the concentration of 100 μg/mL (as shown in Fig. S5). The result demonstrates the UCNP@PDA@AP has high biocompatibility. The finding also manifests that the UCNP@PDA@AP do not induce cell apoptosis.

For demonstrate its ability, the UCNP@PDA@AP is employed for imaging intracellular Cyt *c*. In this case, HepG-2 is arbitrary selected since HepG-2 cells are normally used as a model system for studying substance toxicity and drug metabolism (Rueff et al., 1996). After incubating with the UCNP@PDA@AP in serum-free DMEM for 2 h, the HepG-2 cells exhibit strong UCL emission of UCNPs and weak fluorescence emission of Cy3 (as shown in Fig. 3 column v). This experimental result indicates that the UCNP@PDA@AP can be efficiently uptaken by the HepG-2 cells. The low fluorescence emission of Cy3 is attributed to the spatial isolation of UCNP@PDA@AP with Cyt *c* by the mitochondrial membrane since Cyt *c* is located in mitochondrion of nonapoptotic cells. As a potent apoptosis inducer, etoposide can specifically stimulate the release of cytosolic Cyt *c* from mitochondria (Robertson et al., 2002). As expect, the fluorescence emission of Cy3 is increased with increasing the concentration of etoposide when UCNP@PDA@AP stained HepG-2 cells are incubated with the etoposide. At the same time, the morphology of cells is changed from stretching/adhesive state to shrinkage state with increasing the concentration of etoposide (as shown in Fig. 3). The phenomenon suggests that Cyt *c* is released from mitochondria through etoposide induced cell apoptosis. The result further verifies the practicability of the UCNP@PDA@AP. It is worthy to notice that the UCL signals always exhibit a negligible change with increasing the concentration of etoposide. This phenomenon attributed to the unique optical stability and autofluorescence-free nature of the UCNP, suggesting that UCL signals of UCNP can be used as a potential internal reference to monitor quantitatively intracellular Cyt *c*. For instance, high amount intracellular Cyt *c* leads to high ratio of fluorescence intensity of Cy3 with UCL intensity of UCNP.

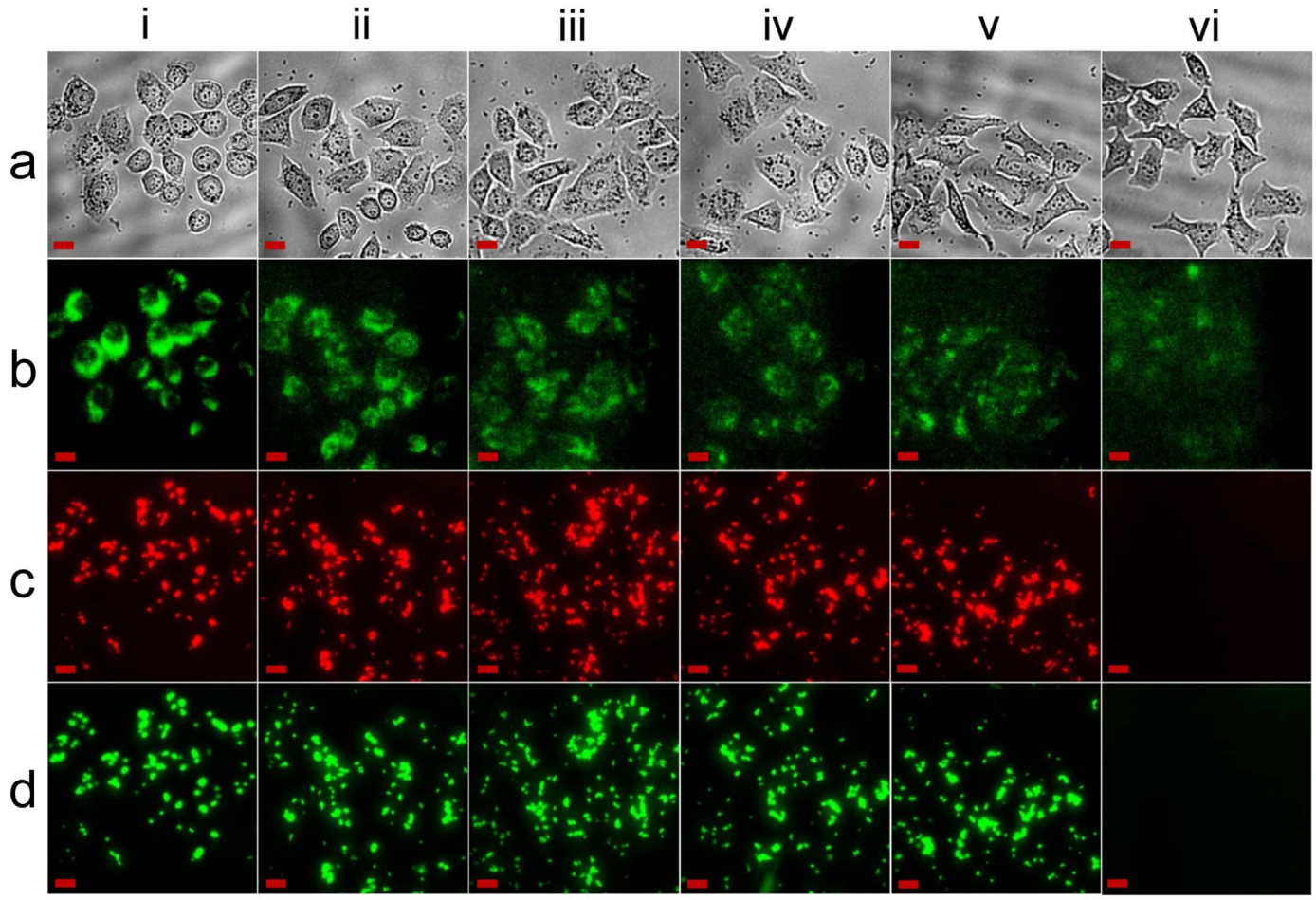

Fig. 3. Fluorescence imaging of UCNP@PDA@AP stained HepG-2 cells treated by various concentrations of etoposide for 2 h. Images are taken from (a) bright-field mode, (b) dark-field mode, (c) the UCL channel (red) and (d) the UCL channel (green), respectively. The concentrations of etoposide are 5 μM (i), 2 μM (ii), 1 μM (iii), 0.5 μM (iv) and 0 μM (v). The blank cells (vi) are used as control sample. The scale bars are 20 μm.

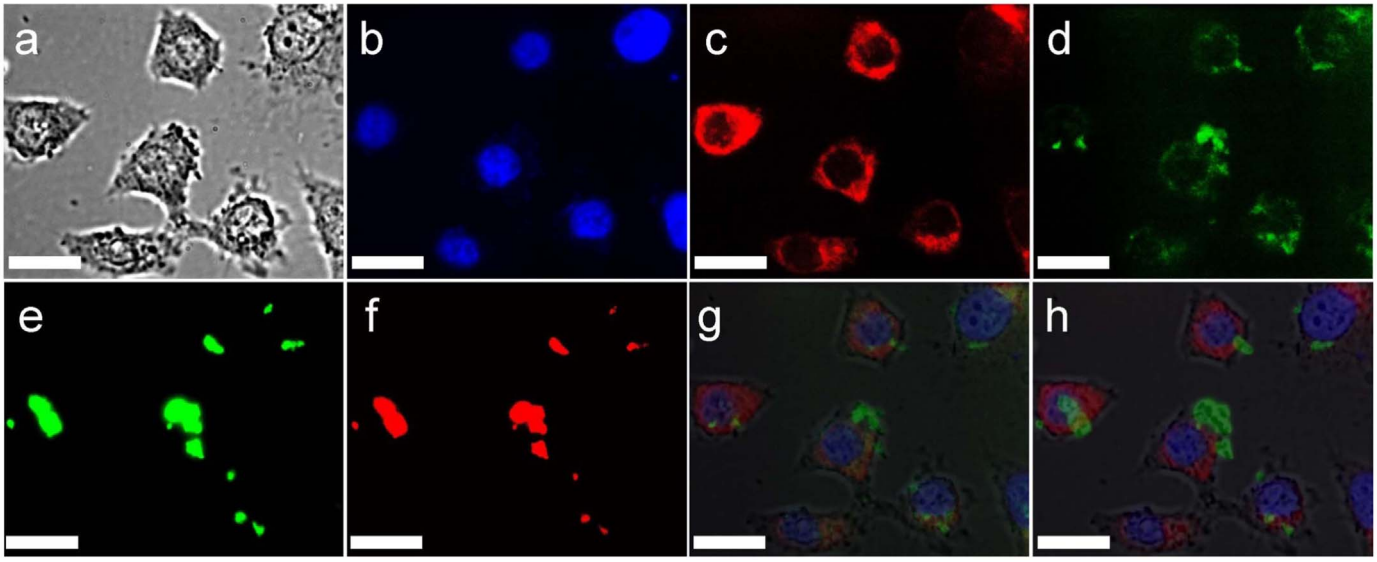

Fig. 4. The fluorescence images for localization analysis of Cyt *c* and UCNP@PDA NPs in HepG-2 cells. Images are taken from (a) bright-field mode, (b) Hoechst 33342 channel (a blue fluorescent dye for labeling the cell nucleus), (c) Mito@tracker channel (a red probe for labeling mitochondria), (d) Cy3 channel, (e) the UCL channel (green) and (f) the UCL channel (red), respectively. (g, h) Merge images of (a, b, c, d) and (a, b, c, e), respectively. The scale bars are 20 μm. (For interpretation of the references to color in this figure legend, the reader is referred to the web version of this article).

The colocalization of Cyt *c* with mitochondria is interrogated to verify that the fluorescence activation response is specific to the release of Cyt *c* from mitochondria into the cytosol. Because the activated fluorescence signal is derived from the aptamer-Cyt *c* complex dissociated from UCNP@PDA@AP surface, the localization of Cyt *c* in the cytosol is able to be visualized by Cy3 imaging. As shown in Fig. 4, the green image appears as a substantially expanded area of the red image, suggesting a diffusion-like release of Cyt *c* from mitochondria. The experimental result is coincided with previous reports (Chen et al., 2015).

3.5. Intracellular quantitation of Cyt c

For quantitative analysis the intracellular Cyt *c*, the UCNP@PDA@AP stained HepG-2 cells were detached from the coverslips and analysed by the fluorescence spectroscopy. The fluorescence intensity of Cy3 is increased with increasing the concentration of etoposide (as shown in Fig. 5a) while the UCL signal of UCNPs keeps as constant during whole experiment (as shown in Fig. S6). The spectral measurements are consistent with the result of fluorescence imaging. On the basis of the assay performance of UCNP@PDA@AP in buffer solution, the intracellular concentration of Cyt *c* can be evaluated by the F_R (as shown in Figs. 5b and S7).

Moreover, the effect of stimulation time on the amount of intracellular Cyt *c* is also investigated while the concentration of etoposide is kept as constant (as shown in Figs. S7–S9). As expected, the fluorescence intensity of Cy3 and F_R are gradually enhanced with increasing the stimulation time, indicating the increased amount of intracellular Cyt *c*. In addition, the result of UCNP@PDA@AP is comparable with the result of the commercial ELISA kit (as shown in Fig. S10). The experimental result confirms that UCNP@PDA@AP could be used to quantitatively evaluate the intracellular Cyt *c*.

4. Conclusions

In summary, an UCNP@PDA core@shell nanoparticle-based fluorescence activated aptameric biosensor (termed as UCNP@PDA@AP)

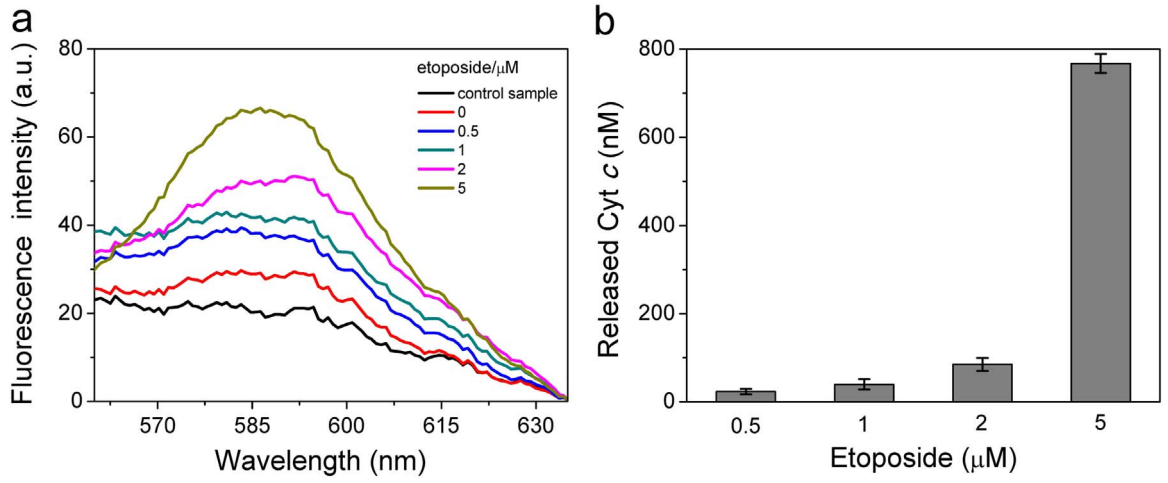

Fig. 5. (a) Fluorescence emission spectra of UCNP@PDA@AP stained HepG-2 cells treated with various concentrations of etoposide for 2 h. (b) Corresponding quantitative analysis of intracellular Cyt *c*. The blank cells are used as control sample. The intracellular concentration of Cyt *c* is evaluated by the F_R (see Figs. 2c and S7). The error bars mean standard deviations ($n=3$).

has been developed for sensing intracellular Cyt *c*. The UCNP@PDA@AP has a detection limit of 20 nM in buffer and is selective toward Cyt *c* compared to the other abundant interferences including HSA. The self-calibrating response of UCNP@PDA@AP with additional positive qualities such as high cellular internalization efficiency and low cytotoxicity, make this nanosensor a unique tool for the qualitative detection of Cyt *c* concentration changes in complex biological matrices and monitoring Cyt *c* mediated cell apoptosis pathway. However, the UCNP@PDA NP also has intrinsic limitations, for example, poor quantum yield of UCNP and relative low loading efficiency of aptamer, which may affect the detection sensitivity of UCNP@PDA@AP. Because of rapid developments in UCNP synthesis methods and biomolecule immobilization strategies, these disadvantages could be overcome in the near future.

Acknowledgement

The authors would like to thank the National Natural Science Foundation of China (Grant No. 21475126) for financial support.

Appendix A. Supplementary material

Supplementary data associated with this article can be found in the online version at http://dx.doi.org/10.1016/j.bios.2016.09.017.

References

Auzel, F., 2004. Chem. Rev. 104, 139–173.
Burns, J.H., 1965. Inorg. Chem. 4, 881–886.
Cao, M., Cao, C., Liu, M., Wang, P., Zhu, C., 2009. Microchim. Acta 165, 341–346.
Chen, T.T., Tian, X., Liu, C.-L.W., Ge, J., Chu, X., Li, Y.F., 2015. J. Am. Chem. Soc. 137, 982–989.
Crouser, E.D., Gadd, M.E., Julian, M.W., Huff, J.E., Broekemeier, K.M., Robbins, K.A., Pfeiffer, D.R., 2003. Anal. Biochem. 317, 67–75.
Degterev, A., Boyce, M., Yuan, J., 2003. Oncogene 22, 8543–8567.
Goldstein, J.C., Munoz-Pinedo, C., Ricci, J., Adams, S.R., Kelwkar, A., Schuler, M., Tsien, R.Y., Green, D.R., 2005. Cell Death Differ. 12, 453–462.
Green, D.R., Kroemer, G., 2004. Science 305, 626–629.
Gu, Z.J., Yan, L., Tian, G., Li, S.J., Chai, Z.F., Zhao, Y.L., 2013. Adv. Mater. 25, 3758–3779.
Guo, T., Deng, Q.L., Fang, G.Z., Liu, C.C., Huang, X., Wang, S., 2015. Biosens. Bioelectron. 74, 498–503.
Haase, M., Schäfer, H., 2011. Angew. Chem. Int. Ed. 50, 5808–5829.
Ju, Q., Tu, D., Liu, Y., Li, R., Zhu, H., Chen, J., Chen, Z., Huang, M., Chen, X., 2012. J. Am. Chem. Soc. 134, 1323–1330.
Li, B., Lu, M.Q., Wang, Q.Z., Shi, G.Y., Liao, W., Huang, S.S., 2015. Chin. J. Anal. Chem. 43, 643–650.
Li, L., Zhang, R., Yin, L., Zheng, K., Qin, W., Selvin, P.R., Lu, Y., 2012. Angew. Chem. Int. Ed. 51, 6121–6125.
Li, L.L., Wu, P.W., Hwang, K., Lu, Y., 2013. J. Am. Chem. Soc. 135, 2411–2414.
Li, P., Peng, Q., Li, Y.D., 2009. Adv. Mater. 21, 1945–1948.
Li, X., Liu, H., He, X., Song, Z., 2010. Appl. Biochem. Biotechnol. 160, 1065–1073.
Li, Z., Zhang, Y., Jiang, S., 2008. Adv. Mater. 20, 4765–4769.
Lin, X.Y., Cui, L., Huang, Y.S., Lin, Y., Xie, Y., Zhu, Z., Yin, B.C., Chen, X., Yang, C.Y.J., 2014. Chem. Commun. 50, 7646–7648.
Liu, F.Y., Zhao, Q., You, H.P., Wang, Z.X., 2013b. Nanoscale 5, 1047–1053.
Liu, F.Y., He, X.X., Liu, L., You, H.P., Zhang, H.M., Wang, Z.X., 2013a. Biomaterials 34, 5218–5225.
Liu, F.Y., He, X.X., Lei, Z., Liu, L., Zhang, J.P., You, H.P., Zhang, H.M., Wang, Z.X., 2015. Adv. Healthc. Mater. 4, 559–568.
Liu, J.M., Yan, X.P., 2011. J. Anal. Spectrom. 26, 1191–1197.
Liu, X., Cao, J., Li, H., Li, J., Jin, Q., Ren, K., Ji, J., 2013c. ACS Nano 7, 9384–9395.
Liu, Y., Tu, D., Zhu, H., Li, R., Luo, W., Chen, X., 2010. Adv. Mater. 22, 3266–3271.
Liu, Y., Zhou, S., Tu, D., Chen, Z., Huang, M., Zhu, H., Ma, E., Chen, X., 2012. J. Am. Chem. Soc. 134, 15083–15090.
Loo, F.C., Ng, S.P., Wu, C.M.L., Kong, S.K., 2014. Sens. Actuat. B-Chem. 198, 416–423.
Luo, D., Huang, J., 2009. Anal. Chem. 81, 2032–2036.
Ma, L.N., Lei, Z., Liu, F.Y., Wang, Z.X., 2015. Sens. Bio-Sens. Res. 3, 92–97.
Mai, H.X., Zhang, Y.W., Sun, L.D., Yan, C.H., 2007. J. Phys. Chem. C 111, 13721–13729.
Martinou, J.C., 1999. Nature 399, 411–412.
Pandiaraj, M., Sethy, N.K., Bhargava, K., Kameswararao, V., Karunakaran, C., 2014. Biosens. Bioelectron. 54, 115–121.
Pandiaraj, M., Madasamy, T., Gollavilli, P.N., Balamurugan, M., Kotamraju, S., Rao, V. K., Bhargava, K., Karunakaran, C., 2013. Bioelectrochemistry 91, 1–7.
Park, Y.I., Lee, K.T., Suh, Y.D., Hyeon, T., 2015. Chem. Soc. Rev. 44, 1302–1317.
Peng, J.J., Wang, X., Chai, L.T., Han, S.Y., Kim, B., Samanta, A., Er, J.C., Wang, L., Yuan, L., Liu, X.G., Chang, Y.-T., 2015. J. Am. Chem. Soc. 137, 2336–2342.
Qian, H.-S., Zhang, Y., 2008. Langmuir 24, 12123–12125.
Qiang, W.B., Li, W., Li, X.Q., Chen, X., Xu, D.K., 2014. Chem. Sci. 5, 3018–3024.
Robertson, J.D., Enoksson, M., Suomela, M., Zhivotovsky, B., Orrenius, S., 2002. J. Biol. Chem. 277, 29803–29809.
Rueff, J., Chiapella, C., Chipman, J.K., Darroudi, F., Silva, I.D., Duverger Van Bogaert, M., Fonti, E., Glatt, H.R., Isern, P., Laires, A., Leonard, A., Llagostera, M., Mossesso, P., Natarajan, A.T., Palitti, F., Rodrigues, A.S., Schinoppi, A., Turchi, G., Werle Schneider, G.,, 1996. Mutat. Res. 353, 151–176.
Shen, Y., Yang, X.-F., Wu, Y., Li, C., 2008. J. Fluoresc. 18, 163–168.
Trusova, V.A., Gorbenko, G.P., Molotkovsky, J.G., Kinnunen, P.K., 2010. Biol. J. 99, 1754–1763.
Uren, R.T., Dewson, G., Bonzon, C., Lithgow, T., Newmeyer, D.D., Kluck, R.M., 2005. J. Biol. Chem. 280, 2266–2274.
del Valle-Mondragón, L., Ramírez-Ortega, M., Zarco-Olvera, G., Sánchez-Mendoza, A., Pastelín-Hernández, G., Tenorio-López, F.A., 2008. Talanta 74, 478–488.
van Beek-Harmsen, B.J., van der Laarse, W.J., 2005. J. Histochem. Cytochem. 53, 803–807.
Wang, F., Liu, X., 2009. Chem. Soc. Rev. 38, 976–989.
Waterhouse, N., Trapani, J., 2003. Cell Death Differ. 10, 853–855.
Zhang, B.L., Luo, Z., Liu, J.J., Ding, X.W., Li, J.H., Cai, K.Y., 2014. J. Control. Release 192, 192–201.
Zhao, Z., Shen, T., Xu, H., 1989. Spectrochim. Acta 45A, 1113–1116.
Zhou, J., Yao, L.M., Li, C.Y., Li, F.Y., 2010. J. Mater. Chem. 20, 8078–8085.